International Journal of Heat and Mass Transfer 115 (2017) 570–580

Contents lists available at ScienceDirect

International Journal of Heat and Mass Transfer

journal homepage: www.elsevier.com/locate/ijhmt

Two-dimensional transient heat conduction in multi-layered composite media with temperature dependent thermal diffusivity using floating random walk Monte-Carlo method

Reza Bahadori [a,*], Hector Gutierrez [a], Shashikant Manikonda [b], Rainer Meinke [b]

[a] The Florida Institute of Technology, Melbourne, FL 32901, USA
[b] Advanced Magnet Lab Superconductivity and Magnetics, Palm Bay, FL 32905, USA

ARTICLE INFO

Article history:
Received 16 March 2017
Received in revised form 21 May 2017
Accepted 15 July 2017

Keywords:
Monte-Carlo
Heat transfer
Composite
Mesh-free
Non-homogeneous
Thermal diffusivity

ABSTRACT

A novel mesh-free Monte-Carlo method for two-dimensional transient heat conduction in composite media with temperature dependent thermal properties is presented. The proposed approach is based on expressing the solution of the transient conductive heat transfer equation, in domains with temperature-dependent material properties, as a combination of two solutions: Bessel functions and integrals of peripheral temperature. The proposed approach is used to solve transient conduction in composite layered materials with temperature dependent thermal diffusivity. Results are compared against others obtained using a conventional finite element approach. Experimental results for heat transfer in a nonhomogeneous domain (composite layered material) are presented to demonstrate the performance of the proposed approach.

1. Introduction

As a numerical technique to simulate physical problems based on statistical methods, the Monte Carlo method has been used for solving complex boundary value problems since 1940. The Monte Carlo approach was used in the late 1940s by Ulam and Von Neuman to solve neutron diffusion problems. Metropolis and Ulam [1] published a seminal paper on the basics of this method in 1949. Since then, the Monte Carlo method (MCM) has been used to solve various heat transfer problems, such as radiative heat transfer [2–4]. The comprehensive simulation of the thermal behavior of different materials, particularly in the nanoscale [5–9] is another application of this method. [10] describes the floating random walk Monte Carlo method as a mesh free approach to solve conduction in domains with complex geometries, providing computational advantage over finite element or finite difference methods. Another attractive feature of MCM is that it is very well suited to parallel computing. In [11], performance of the random walk method and floating random walk method are compared in solving heat conduction in a domain with homogenous diffusivity, and the ability of using parallel computing and MCM to solve this problem is shown. Haji Sheikh and Sparrow [10] introduced the Monte-Carlo solution of transient heat conduction based on Bessel functions relating time and step length for each particle's floating random walk. Their method calculates the temperature of each point by simply averaging the particles' temperature receiving by the respective point, and is applicable to homogenous media. Burmeister [12] reported the floating random walk Monte-Carlo approach to tackle steady state heat conduction problems in composite media with temperature dependent material properties. The study presented in this paper introduced modifications in both methods and combine them to address transient heat conduction in composite media with nonlinear (temperature dependent) thermal diffusivities, such as composite structures with insulation layers that lead to abrupt changes of diffusivity between layers, as found when modeling superconducting coils.

2. Conductive heat transfer in non-homogeneous media

Phonon heat transfer is described as the emission of energy particles (phonons) from the heat sources to the sinks - the step length from source to sink being therefore a critical parameter to calculate heat transfer. There are some methods [13,14] that have simulated the direct process of phonon transfer (source to sink) using the source's thermal properties. It is possible to use the sink's known

* Corresponding author.
E-mail addresses: rbahadori2013@my.fit.edu (R. Bahadori), hgutier@fit.edu (H. Gutierrez), smanikonda@amlsm.com (S. Manikonda), rbmeinke@amlsm.com (R. Meinke).

http://dx.doi.org/10.1016/j.ijheatmasstransfer.2017.07.071
0017-9310/

thermal properties to estimate the location of the sources that can transfer the phonon in the defined time span to the sink. In this paper, the latter approach is used.

The concept of heat transfer between source and sink follows the potential theory and consequently can be solved using polar coordinate system. Therefore, an infinite cylinder with radius r and initially kept at the zero temperature is set as initial version of problem [15]. For $\tau > 0$, the temperature of the boundary is set to $T(r, \theta, \tau)$. The temperature at the centerline of a cylinder can be obtained by solving the convolution integral [10,16]:

$$T(x, y, t) = \int_{\tau=0}^{t} \int_{F=0}^{1} T(r, \theta, t - \tau) dF dH^{(2)} \tag{1}$$

$$F(\theta) = \frac{\theta}{2\pi}, H^{(2)}\left(\frac{\alpha\tau}{r^2}\right) = 1 - 2\sum_{k=0}^{\infty} \frac{\exp\left(-\frac{\Lambda_k^2 \alpha\tau}{r^2}\right)}{\Lambda_k J_1(\Lambda_k)} \tag{2}$$

where Λ_k is root of the Bessel function $J_0(\Lambda)$ and α the thermal diffusivity of the material. As described in [10], the step length (or radius) is the minimum distance to the boundary and the elapsed time τ is accordingly calculated; therefore, the time step is floating in this algorithm. The time step τ needed for each spatial step can be calculated using probability function $H^{(2)}$. Inverse distribution functions for 2D case are [16]:

$$\begin{aligned} \frac{\alpha\tau}{r^2} &= D_1 + D_2(RN) + D_3(RN) + \ldots \quad RN < 0.6 \\ \frac{\alpha\tau}{r^2} &= -0.17292 \ln[0.62423(1 - RN)] \quad RN \geqslant 0.6 \end{aligned} \tag{3}$$

Table 1
Inverse probability functions for floating random walk.

RN	*0.0–0.1*	*0.1–0.3*	*0.3–0.6*
D_1	0.013120	0.052654	0.051155
D_2	3.3082	0.36498	0.35391
D_3	−91.011	−0.45109	−0.33104
D_4	1348.1	0.66164	0.44125
D_5	−9524.2	–	–
D_6	25594	–	–

Ds are coefficients presented in Table 1 and *RN* is replaced by random numbers generated from 0 to 1.

Having fixed radius, minimum distance to the boundary, thermal diffusivity α and $\frac{\alpha\tau}{r^2}$ from (3), floating time step τ can be calculated.

The first proposed modification to the method presented above is fixing the time step and using $H^{(2)}$ to obtain the radius of each circle for the next step. This is necessary to calculate the temperature at the desired time step for all points - in other words, it is not mandatory for the generated circle to touch the closest boundary. The next step is the generation of a random number to use in the angular distribution function $F(\theta)$, and pass the particles from the source aligning the generated angle and as far as the calculated step length. Figs. 1 and 2 depict the particle propagation after one iteration using the floating random walk method from [10] before and after the modification.

The second proposed modification allows consideration of non-homogenous thermal diffusivity in the calculations. Although α, the thermal diffusivity of the sink in Eq. (2) affects the step length directly, it cannot consider the change of diffusivity along the path that the particle follows from source to sink. In [17–20], modifications to the original random walk Monte Carlo method have been proposed to account for the change of thermal properties in the medium; however, meshing is required in these approaches. In [21,22], the random walk Monte-Carlo method for diffusion in spatially non-homogenous medium is studied – this can be adapted and used in a floating random walk method proposed in this paper. This is possible provided that the function describing the spatially dependent thermal diffusivity is available. For a linear change in thermal diffusivity and knowing the positions of both source and sink, this function can be calculated; however, in media with non-linear thermal diffusivity, it may be difficult to extract the diffusivity function in each time step. In composite materials consisting of thermal insulators, the diffusivity function is similar to a step function. Modification methods for step length that use derivatives to calculate the rate of change of diffusivity can introduce significant errors in the numerical calculation of step function slopes. Hence, a new algorithm is required to adjust the step length.

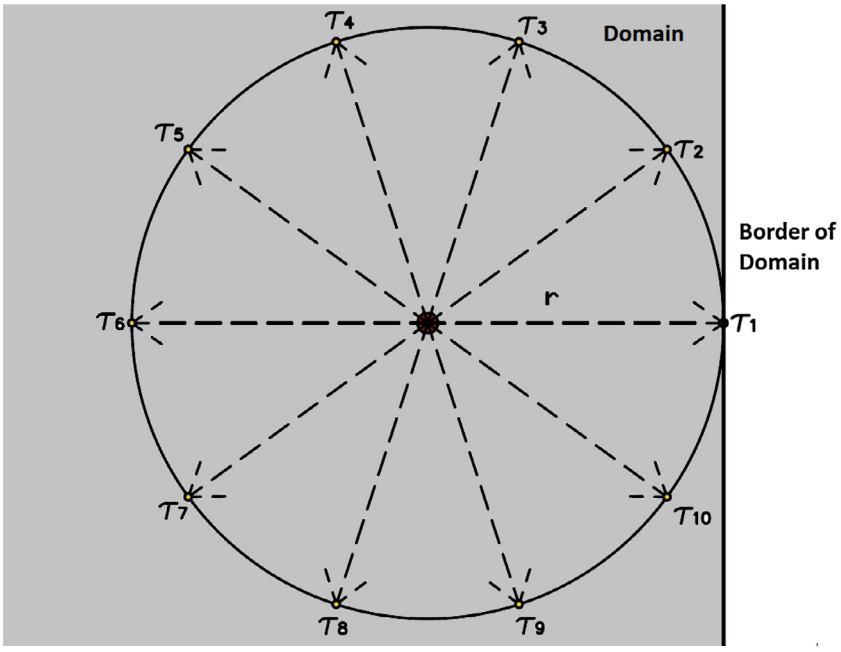

Fig. 1. Floating random walk (FRW) with fixed step length for each iteration and floating time steps.

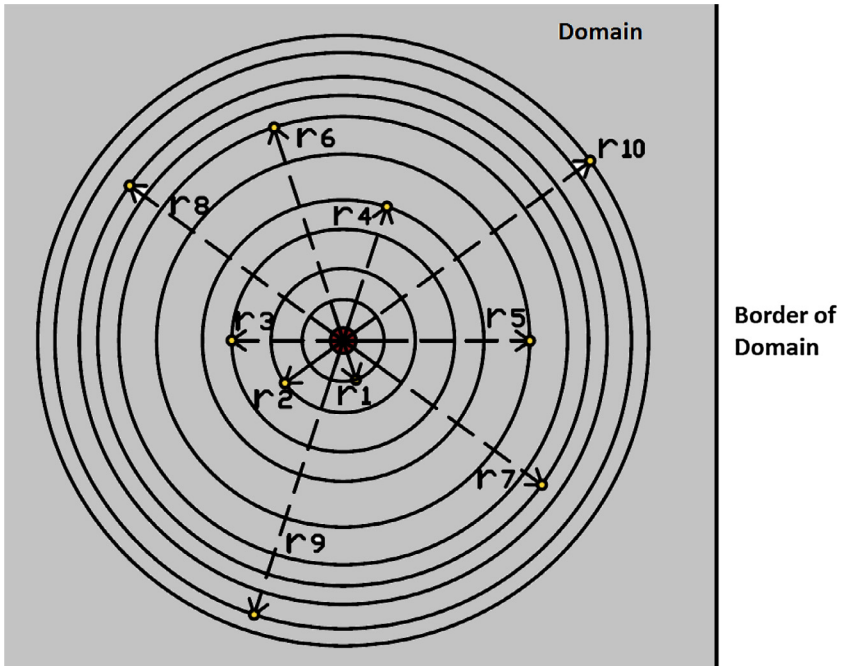

Fig. 2. Modified FRW with floating step length for each iteration and fixed time step.

As an example, consider a square shape copper plate with side length 0.2 and initial (uniform) temperature of 27 K at time $t = 0$. The middle of the plate experiences a change in temperature of 77 K in a rectangular area with side length = 0.06 m. For > 0, the borders of the plate are kept at the fixed temperature of 27 K. Fig. 3 shows the diffusivity of the copper plate in the initial condition, where the diffusivity of each point has been interpolated based on the diffusivity of copper as function of temperature shown in Fig. 4. The yellow dot near the hotter spot is the k^{th} point out of K points distributed in the domain, in this case $K = 10,000$. The diffusivity around point k is not homogenous and experiences a step function change. This effect shall be included in the computation of step length to obtain accurate temperature distribution.

The probability distribution function $H^{(2)}$ can be acquired from the fit functions in [16]. The result is:

$$\frac{\alpha\tau}{r^2} = C \tag{4}$$

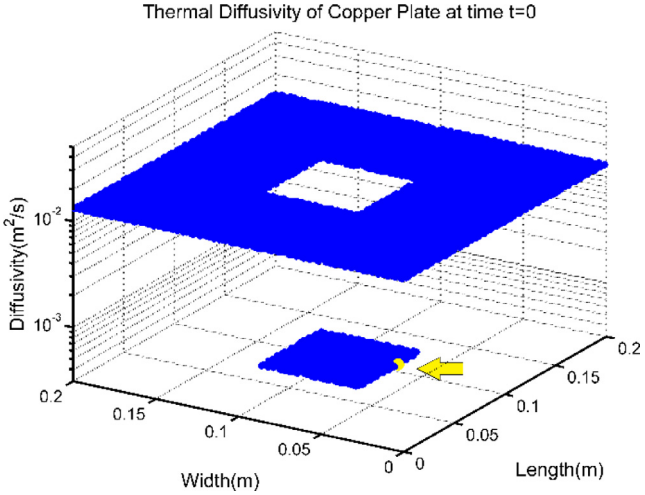

Fig. 3. The thermal diffusivity of the copper plate the initial condition.

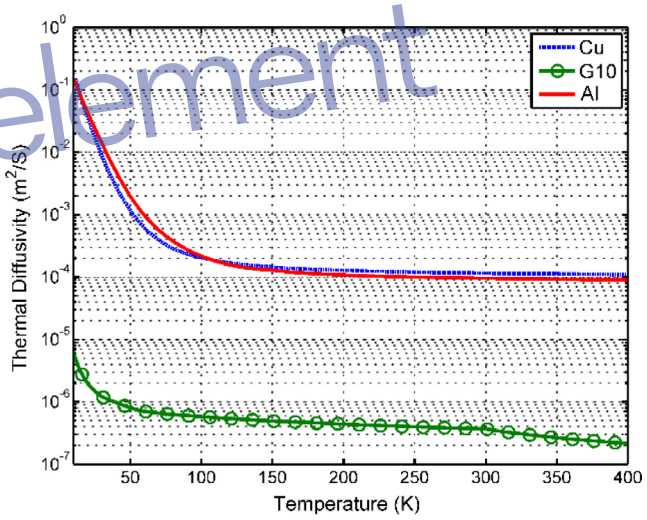

Fig. 4. Thermal diffusivity of copper as function of temperature.

where C is a generated random number substituted into the fit functions. The steplength r can be calculated as:

$$r = \sqrt{\frac{\alpha dt}{C}} \tag{5}$$

This solution is accurate for media with homogenous diffusivity. To model domains with nonlinear diffusivity such as copper (Fig. 3), the generated path r is divided in M smaller steps, and the total modified step length can be calculated as:

$$r_j = \sum_{m=1}^{M} r_m = \sum_{m=1}^{M} \sqrt{\frac{\alpha_m dt}{CM^2}} \tag{6}$$

where the index $1 \leqslant m \leqslant M$ denotes the location of the j^{th} particle after passing each sub step length:

$$\begin{aligned} x_{m+1} &= x_m + r_m \cos(\theta_j) \\ y_{m+1} &= y_m + r_m \sin(\theta_j) \end{aligned} \tag{7}$$

For $m = 1$, the diffusivity of the center point k will be used in Eq. (6), $\alpha_1 = \alpha_k$; and $x_1 = x_k$, $y_1 = y_k$ represent the particle location at $t = 0$. For $m > 1$, the thermal diffusivity is extracted by interpolation from Fig. 4, relative to the temperature at the particle location .The final location of the particles after each time step can be calculated as:

$$\begin{aligned} x_j &= x_k + r_j \cos(\theta_j) \\ y_j &= y_k + r_j \sin(\theta_j) \end{aligned} \tag{8}$$

The j index accounts for the particle number (out of J particles emitted from points denoted by the k index), and t is the corresponding time index. Figs. 5, 6 show all sub-step length locations of $J = 1000$ particles emitting from the k^{th} point shown in Fig. 3 as a yellow spot, when M is equal to 10 at time step t = 1, before and after applying the step length modification. The initial temperature of the mentioned point is 77 K. The length and width shown in Figs. 5 and 6 are the copper plate dimensions. The effect of the change in thermal diffusivity along the path can be seen in Fig. 6 as longer step lengths for particles moving towards the area with lower temperature (27 K), where points have higher thermal diffusivity. The color bar shows the thermal diffusivity at each sub step length.

Using modified step lengths, each particle adopts the temperature of the domain at the particle's location. The following boundary conditions apply to particles falling in or out of the boundary in each time step:

1. Fixed temperature boundary condition: the particles adopt the pre-assigned fixed temperature of the boundary.
2. Insulation boundary condition: the particles adopt the temperature of the sink.

The third kind of boundary condition (convection boundary condition) has not been addressed in this paper. The calculation of temperature at each point follows the same procedure as in homogenous medium:

$$T^{t+1}_{(x_k,y_k)} = \frac{1}{J}\sum_{j=1}^{J} T^{t}_{(x_j,y_j)} \tag{9}$$

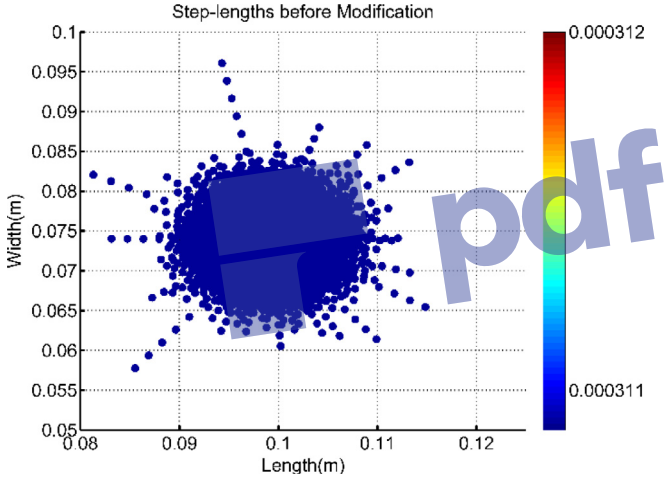

Fig. 5. Step length with the central diffusivity of the sink.

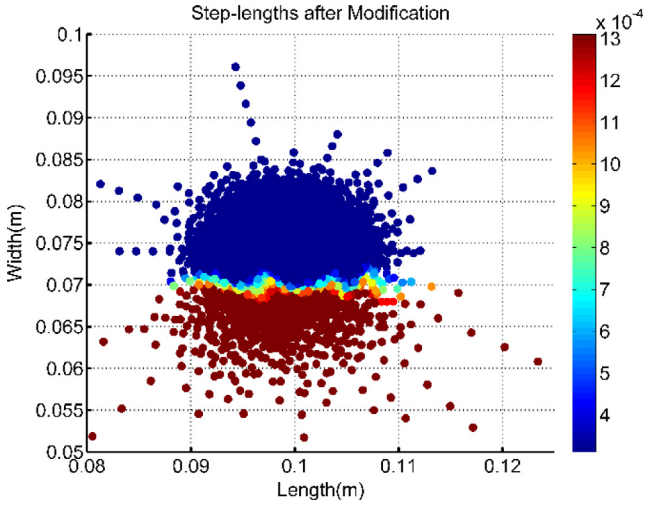

Fig. 6. Modified step length with path diffusivity.

3. Composite-layered materials with non-homogeneous thermal properties

The formulation presented above can tackle the problem of a single media with non-homogenous material properties. When the media consists of composite layers where each layer has non-homogenous temperature dependent material properties, further modifications in Eq. (9) are required to calculate the temperature of the centerline in cylindrical coordinates. The third modification here proposed takes the thermal diffusivity of peripheral particles into account to calculate the centerline temperature of the cylinder; or in other words, the temperature at the point. Ref. [12] proposed a method to solve this problem as a steady state heat conduction problem. The steady state equation of heat conduction for infinite cylinder with non-homogenous thermal conductivity can be written as:

$$\frac{1}{r}\frac{\partial\left(k(r,\theta) r \frac{\partial T(r,\theta)}{\partial r}\right)}{\partial r} + \frac{1}{r^2}\frac{\partial\left(k(r,\theta)\frac{\partial T(r,\theta)}{\partial \theta}\right)}{\partial \theta} = 0 \tag{10}$$

Since the same conditions apply at the beginning and end of the traverse, integration of this equation with respect to θ from 0 to 2π, makes the second expression equal to zero.

$$\int_0^{2\pi} \frac{1}{r^2}\frac{\partial}{\partial\theta}\left(k(r,\theta)\frac{\partial T(r,\theta)}{\partial\theta}\right) d\theta =$$

$$\frac{1}{r^2}\left(k(r,2\pi)\frac{\partial T(r,2\pi)}{\partial\theta} - k(r,0)\frac{\partial T(r,0)}{\partial\theta}\right) = 0 \tag{11}$$

Integration from 0 to r yields:

$$\int_0^{r} \frac{\partial\left(\int_0^{2\pi} k(r,\theta) r \frac{\partial T(r,\theta)}{\partial r} d\theta\right)}{\partial r} dr =$$

$$\int_0^{2\pi} k(r,\theta) r \frac{\partial T(r,\theta)}{\partial r} d\theta = 0 \tag{12}$$

In the steady state, time is not a variable in the partial differential equation and therefore particles have a perfect circular distribution around the center point. However, in the transient case there is a nonlinear relationship between the time step and step length (2), so the distribution of particles does not follow a perfect circle and, unlike [12], r cannot be omitted from (12). Introducing the coordinate transformation in (13) and (14), $T(r,\theta)$ will be defined in terms of $T(\eta,f)$.

$$\eta = \frac{\int_0^{r} \frac{dr'}{k(r',\theta) r}}{\int_0^{R} \frac{dr'}{k(r',\theta) r}} \tag{13}$$

$$f = \frac{\int_0^{\theta} \frac{d\theta'}{\int_0^R dr'/k(r',\theta')r}}{\int_0^{2\pi} \frac{d\theta}{\int_0^R dr'/k(r',\theta)r}} \tag{14}$$

It should satisfy the total differential relationship:

$$dT(r,\theta) = dT(\eta,f) \Rightarrow \frac{\partial T(r,\theta)}{\partial r}dr + \frac{\partial T(r,\theta)}{\partial \theta}d\theta = \frac{\partial T(\eta,f)}{\partial \eta}d\eta + \frac{\partial T(\eta,f)}{\partial f}df \tag{15}$$

This implies:

$$\frac{\partial T(r,\theta)}{\partial r}dr = \frac{\partial T(\eta,f)}{\partial \eta}d\eta \tag{16}$$

Using (13), $d\eta$ can be defined as shown in (17). A, B, $I_{2\pi}B$ and I_RA are used to simplify the representation of numerator and denominator in the next steps.

$$d\eta = \frac{\frac{1}{k(r',\theta)r}}{\int_0^R \frac{dr'}{k(r',\theta)r}}dr' = \frac{A}{I_RA}dr' \Rightarrow \frac{\partial T(r,\theta)}{\partial r} = \frac{\partial T(\eta,f)}{\partial \eta}\frac{A}{I_RA} \tag{17}$$

In the next step, $d\theta$ is calculated as:

$$df = \frac{\frac{1}{\int_0^R \frac{dr'}{k(r',\theta')r}}}{\int_0^{2\pi} \frac{d\theta}{\int_0^R \frac{dr'}{k(r',\theta')r}}}d\theta' = \frac{B}{I_{2\pi}B}d\theta' \Rightarrow d\theta = \frac{I_{2\pi}B}{B}df \tag{18}$$

Substituting (17) and (18) in Eq. (12) yields:

$$\int_0^{2\pi} \frac{1}{A}\frac{\partial T(\eta,f)}{\partial \eta}\frac{A}{I_RA}\frac{I_{2\pi}B}{B}df = 0 \tag{19}$$

Note that, $k(r,\theta)r = \frac{1}{A}$, $I_RA = \frac{1}{B}$ and $I_{2\pi}B = Constant$. Eq. (12) can be written after transformation as:

$$\int_0^1 \frac{\partial T(\eta,f)}{\partial \eta}df = 0 \tag{20}$$

After integrating with respect to η from 0 to the outer radius for each particle, Eq. (20) can be written as (21). T_c is centerline temperature and T_R is the peripheral temperatures:

$$\int_0^1 (T_R - T_C)df = 0 \tag{21}$$

Substituting Eqs. (18) in (21) yields the centerline temperature as presented in (22).

$$T_C = \frac{\int_0^{2\pi} \frac{rT(R,\theta)}{\int_0^R dr'/\alpha(r',\theta)}d\theta}{\int_0^{2\pi} \frac{r}{\int_0^R dr'/\alpha(r',\theta)}d\theta} \tag{22}$$

Discretizing the problem numerically allows the use of the method proposed in [12] for the transient case by the estimate of using thermal diffusivity instead of thermal conductivity. It should be noted that radius r for each angle θ is constant and can come out of internal integral and result in (22). Figs. 7 and 8 depict the participating variables in the centerline temperature before and after the proposed modification, respectively. Due to the transient effect, there will be a contour shape of particles around the centerline instead of a perfect circular shape as seen in the steady state. Eq. (22) holds for both non-homogenous and composite media. It can be used instead of equation (9) for single non-homogenous media as well.

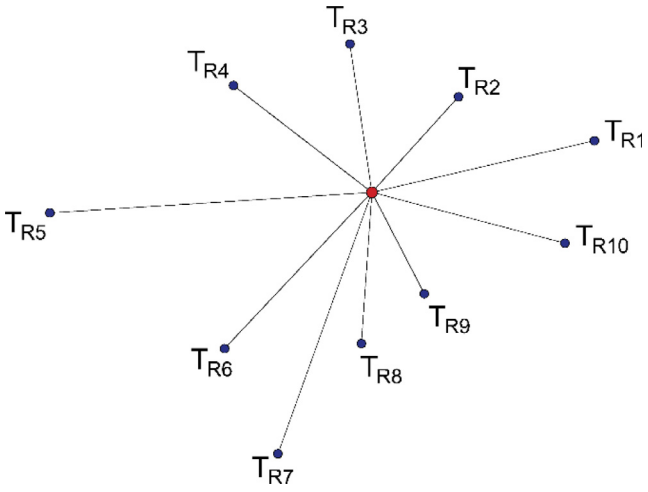

Fig. 7. Participating variables in T_C before modification, Eq. (9).

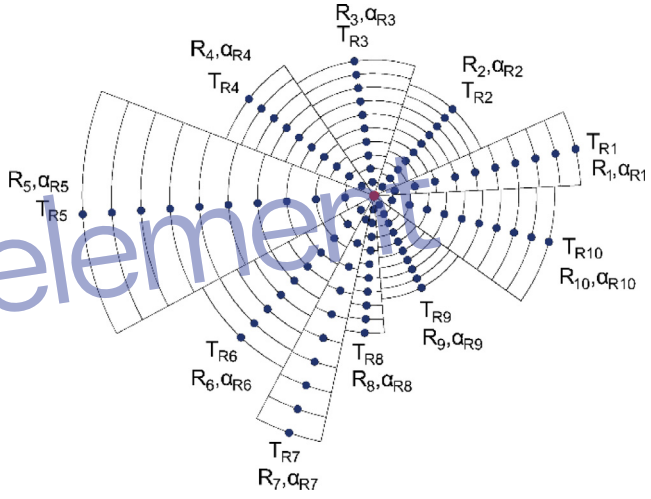

Fig. 8. Participating variables in T_C after Modification, equation (22).

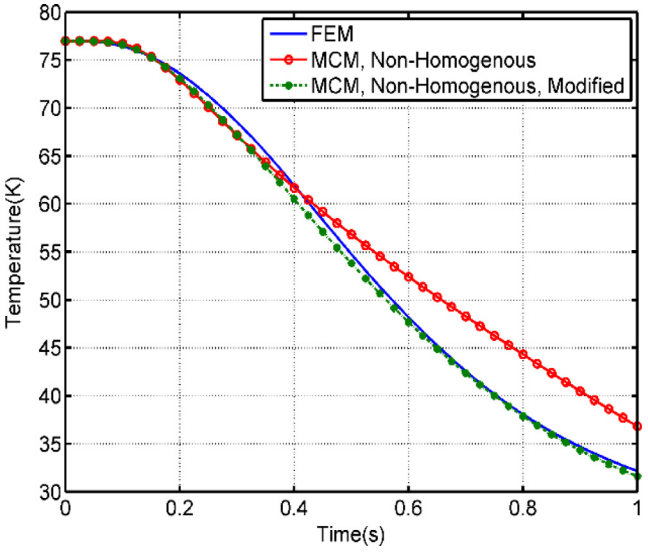

Fig. 9. Comparison of floating random walk simulation (before and after modification) with FEM, for peak temperature during a 1-s simulation of a copper plate considering non-homogenous diffusivity.

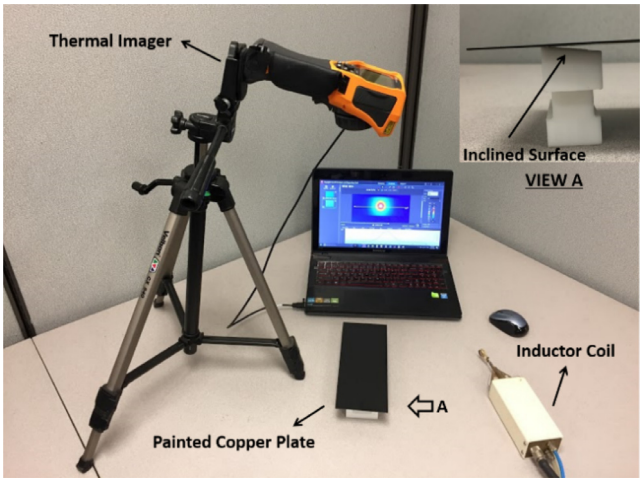

Fig. 10. Test setup using a thermal imager.

The number of particles J in Figs. 7 and 8 emanated from the sink is 10, and each particle path has been divided in ten substeplengths in Fig. 8 ($M = 10$).

4. Results for single material non-homogeneous media compared to those obtained by finite element methods

To verify the proposed method (modified floating random walk, MCM) to model heat conduction in a medium with non-homogenous thermal diffusivity, the copper plate example described above has been implemented in commercial FEM software (ANSYS) to compare results. The number of nodes in the FEM model are adjusted to match the number of points used in MCM. Fig. 9 shows the temperature change of the point at the middle of the plate starting at T = 77 K during 1 s using three methods:

1. Monte-Carlo method before modification. Step length is calculated using $r_j = \sqrt{(\alpha_j)dt/C}$, and centerline temperature is calculated as shown in [10].
2. Modified MCM, where Eq. (6) is used for step length calculation and Eq. (22) is used to estimate centerline temperature.
3. Finite element ANSYS model: nonlinear simulation of transient heat conduction, taking temperature- dependent material properties into account.

5. Verification of results for single material non-homogeneous medium vs measurements

Fig. 10 shows the test setup for measurement of temperature distribution in a copper plate using a thermal imager. The thermal imager is KEYSIGHT U5855A, and has a sensitivity of ±0.1 °C and accuracy of ±2 °C. The resolution of the thermal imager screen is 320 × 240 pixels. The thermal imager was set to capture 8 frames per second during the test. The copper plate's length and width are approximately 262 mm and 109 mm, respectively. The thin copper plate has a thickness of roughly 0.6 mm, which makes the two

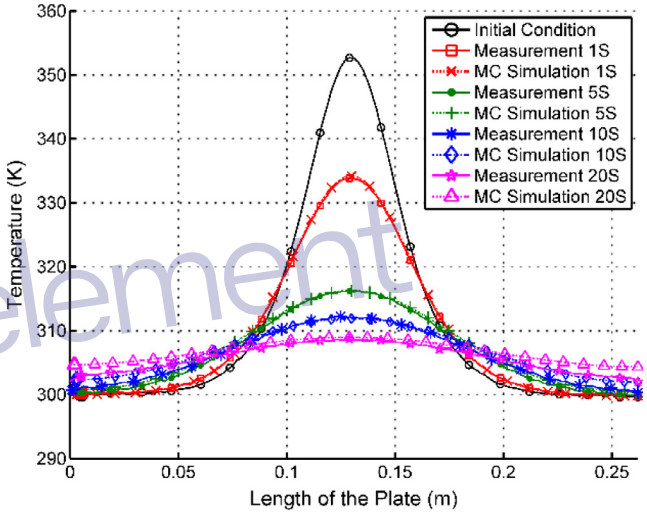

Fig. 12. MCM Simulation vs measurements for copper plate.

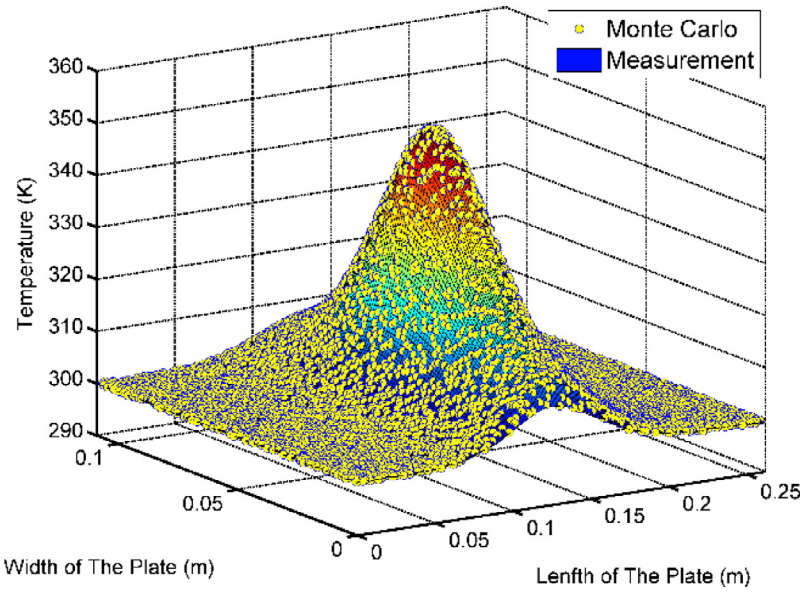

Fig. 11. The initial condition for the MC simulation was extracted from a thermal image of the plate.

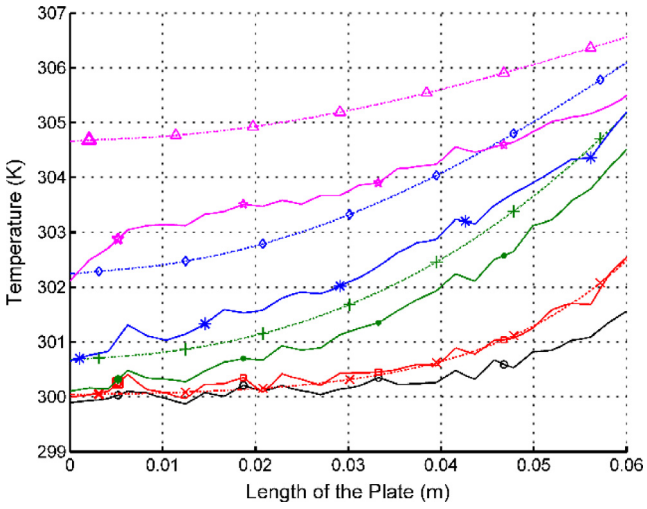

Fig. 13. Comparison of MCM simulation vs measurement for the copper plate, close to the boundary.

dimensional simulation a reasonable approximation for comparison with this test.

VIEW A shows the painted copper plate resting on plastic holders. The top surface of the holders is inclined to minimize the conduction heat transfer by contact between the copper plate and holders. Flat black paint is used on both sides of the copper plate to minimize the reflectivity of the surface – the readings are therefore mostly given from emissivity of the copper plate. The emissivity is set to 0.95 in the thermal imager. The painting not only increases the measurement accuracy of the thermal imager but can also reduce the impact of convection heat transfer on the test. This also makes insulation boundary condition more reasonable approximation in simulation. Using an inductive heating system, the center of the copper plate was heated up and then the induction coil was removed from the top of the plate. The induced heat transfers through the plate until the entire plate reaches a uniform temperature. The transient process is captured at 8 frames/s by the thermal imager. The initial condition for the Monte Carlo simulation comes from the first image after removing the coil. Fig. 11 shows the measurement image used as initial condition for the MCM simulation (yellow points). The captured image consists of $253 \times 101 = 25,553$ pixels.

The measured temperature has been interpolated by 6000 randomly distributed points throughout the plate represented by yellow circles. These points are used as initial condition for the MCM simulation. One thousand particles are emitting from each point, and each step length has been divided into $M = 10$ step lengths. A transient Monte-Carlo heat conduction simulation was done for a total time of 20 s. The time step of the simulation was set to 0.125 s to match the thermal imager's frame rate (8 frames/s). Fig. 12 shows the temperature profile of the copper plate's centerline drawn along the length of the plate, i.e., a line drawn from $(0, 0.055)$ to $(0.262, 0.055)$ relative to the coordinates shown in Fig. 11. Simulation results are compared to measurements at time equal to $t = 1, t = 5, t = 10, t = 20$ seconds.

As shown in Fig. 13, the deviation of the simulation respect to the measurements is larger near the boundaries of the plate. Although painting the copper plate alleviates the effect of convection in the measurements, it cannot be fully eliminated. On the other hand, the simulation is done with insulation boundary condition, and for this reason the simulated temperature close to the boundaries is higher than the measurements. Furthermore, this deviation increases with time, which supports the fact that this is a convective effect. This test could be performed in a vacuum chamber, or a third kind of boundary condition (convection) could be introduced to address this deviation.

The probabilistic error of MCM has direct relationship with the number of random walks. A low number of random walk results in higher error. The required number of random walks is related to both the number of points needed to describe the geometry and the number of particles emitting from each point when performing the integration presented in (22). Fig. 14 (left y-axis) shows the convergence of MCM to the measured maximum temperature after 1 s as function of the number of points, while the right y-axis shows the simulation error, also as function of the number of points. After 10k points there are no significant changes, however, after 2k points the% error already falls very close to zero. The number of particles in this study was 1k, and $M = 10$.

The impact of the number of particles on convergence and error propagation in the copper plate example is shown in Fig. 15, using 10k points. This study suggests that 50 particles emitting from

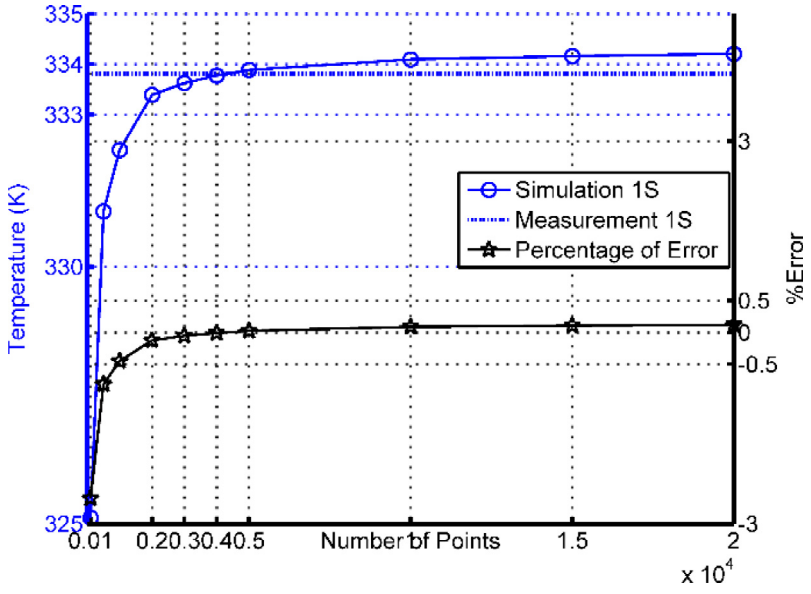

Fig. 14. Percentage of error versus number of points.

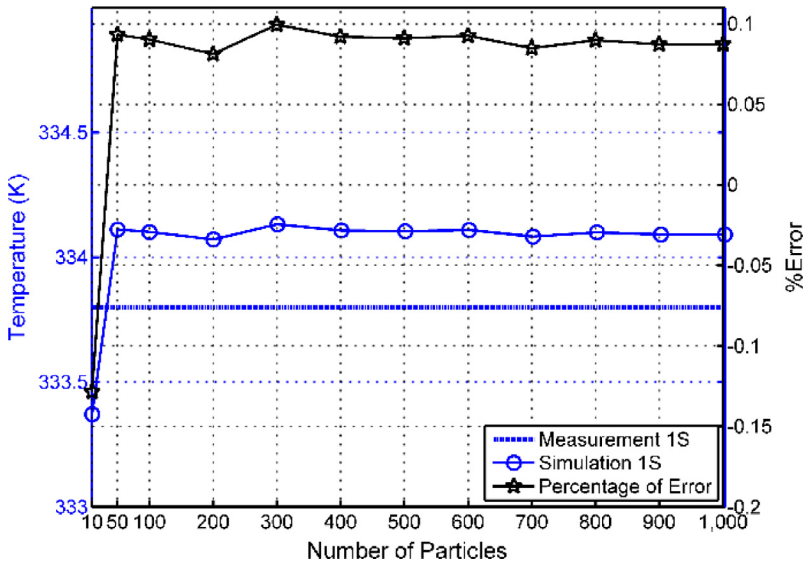

Fig. 15. Percentage of error versus number of particles, using 10 k points.

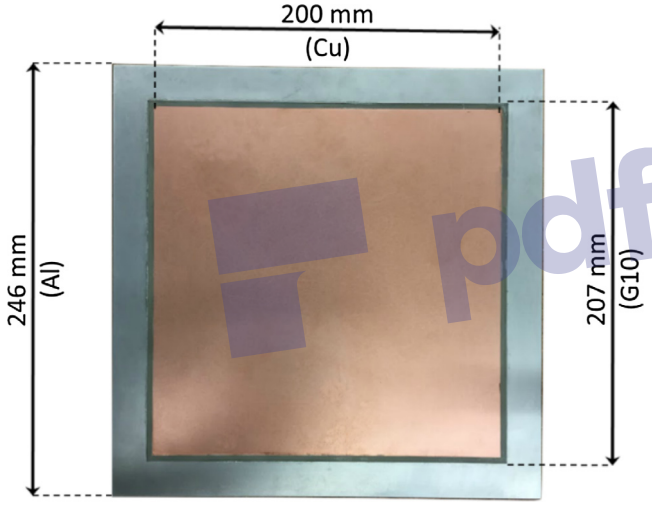

Fig. 16. Composite plate structure ad dimensions.

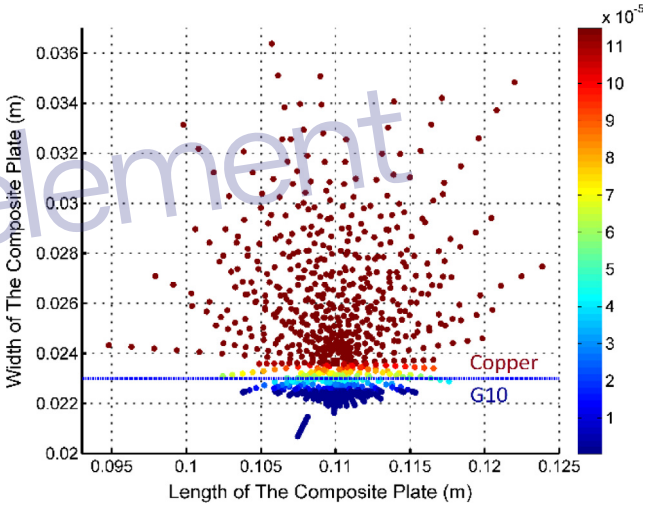

Fig. 17. Scattering of particles in the composite plate assembly using path's diffusivity introduced in (6).

each point is sufficient to properly describe material properties and temperature profile, and leads to less than 0.1 percent error in the integration of (9) for the center point temperature.

6. Verification of results for composite non-homogeneous medium

To verify the simulation results of the proposed mesh free Monte-Carlo method for two-dimensional heat conduction in a composite layered structure with temperature dependent material properties, a test was designed to capture and measure the transient temperature distribution due to heat conduction in a composite plate shown in Fig. 16. A frame made of G10 composite with side length of 207 mm inscribes a rectangular copper plate with side length of 200 mm, leaving 3.5 mm of G10 as thermal insulation layer around the copper plate. A second frame made of aluminum, with side length of 246 mm, surrounds the assembly of G10 and copper leaving a 19.5 mm strip of aluminum as outermost layer of the composite structure.

The experiment using this composite assembly was similar to the copper plate example, and the setup is the same as shown in Fig. 10. Using the inductive heating system, the middle of the copper plate in the innermost layer of the assembly was heated up, and after removing the inductor, the first image captured by the thermal imager was fed to the MCM simulation as initial condition. The surface of the assembly shown in Fig. 16 was painted flat black to improve the emissivity reading of the test specimen and have a more accurate temperature reading by the thermal imager.

The material properties of copper, aluminum and G10 used in the MCM simulation are shown in Fig. 4, as extracted from the Cryocomp software and NIST website. Fig. 17 depicts 100 scattered particles from a point located in copper near the edge of G10. Each step length has been divided in 10 sub-step lengths using Eq. (6). The impact of the path's thermal diffusivity can be seen in the figure, as longer step lengths are seen in copper (where thermal diffusivity is higher) than in the lower layer made of G10.

The initial condition in the MC simulation of the composite assembly was obtained from measurement using the thermal imager. Fig. 18 shows the initial condition captured by the thermal imager and fed to the simulation.

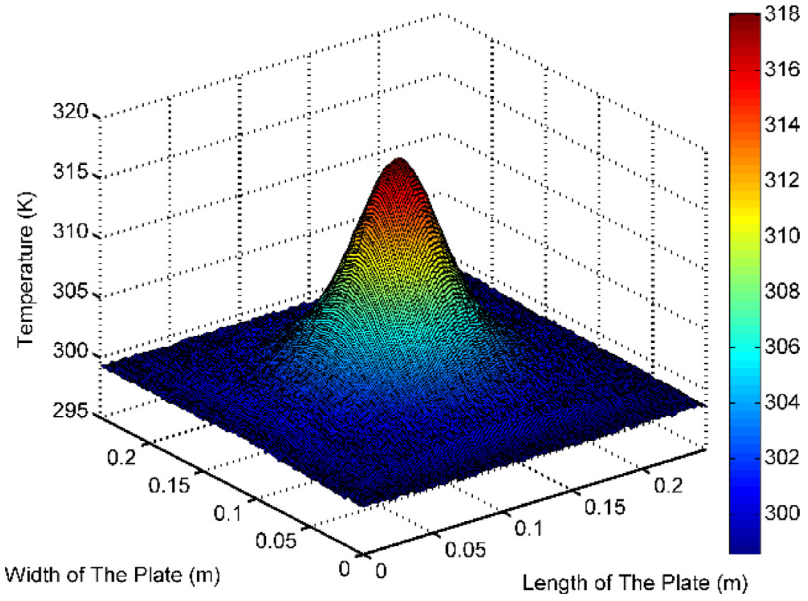

Fig. 18. Initial condition for CM simulation captured by thermal imager.

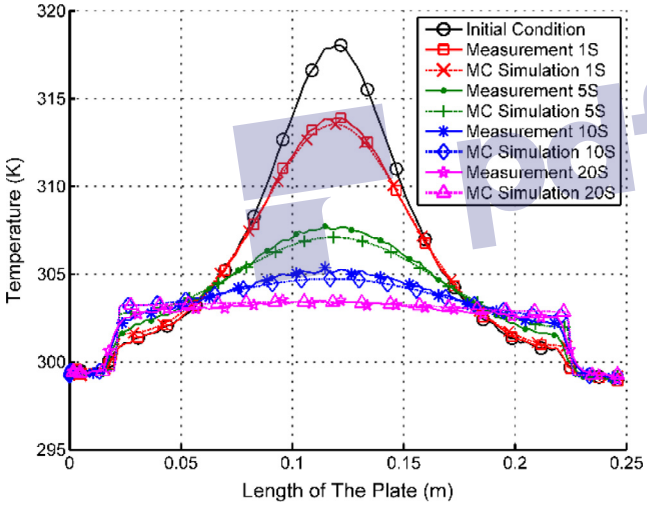

Fig. 19. MCM Simulation vs measurement for the composite plate.

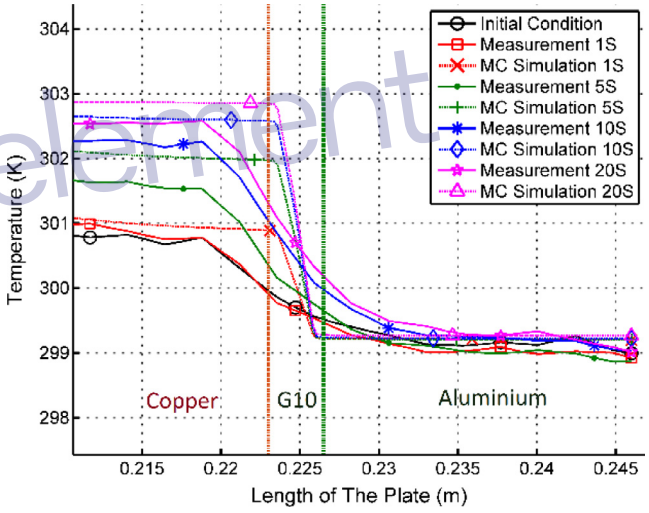

Fig. 20. MCM Simulation vs measurement for the composite plate near the boundary.

Time step is set to 0.125 s to match the frame rate of the thermal imager (8 frames/s). The temperature profile of the composite plate's centerline is presented for both simulation and measurement in Fig. 19. The comparison is done at time steps $t = 1, t = 5, t = 10, t = 20$ s. The agreement between simulation results and measurements confirms the ability of the proposed Monte-Carlo method in predicting transient thermal conduction in a composite layered structure with temperature dependent material properties.

Fig. 20 is a zoomed plot of the area close to the right boundary of the composite plate. From left to right on the plot, the temperature profile when transitioning from copper to G10 to aluminum can be compared for both MC simulation and measurement. The MC simulation shows steep transitions in the temperature profile (similar to a step function) while the thermal imager shows a smoother transition between different layers. The difference in transitions roots in the limitation of the thermal imager to capture accurately temperature changes when the temperature experiences a step function profile. G10, acting as insulation layer between copper and aluminum, prevents heat to transfer from copper to the aluminum and produces a slump in the temperature profile. The MC simulation correctly predicts the impact of G10 in the transient heat conduction, yielding approximately a step function temperature profile in the respective area. Due to the mixture of infrared waves from different materials (copper, G10 and aluminum) with very different frequencies due to a step temperature difference, the thermal imager produces an inaccurately smooth temperature transition profile in this area. Fig. 21 illustrates the aforementioned limitation of the thermal imager.

To verify this shortcoming on the thermal imager, an experiment was developed to assess the ability of the thermal imager to accurately measure a known step function temperature change between two materials. Fig. 22 shows the experimental setup, consisting of two plastic pillars and one copper block in between. While the plastic pillars are at room temperature, the copper block is cooled down with ice to approximately $T = 0\,^{\circ}\mathrm{C}$. The thermal

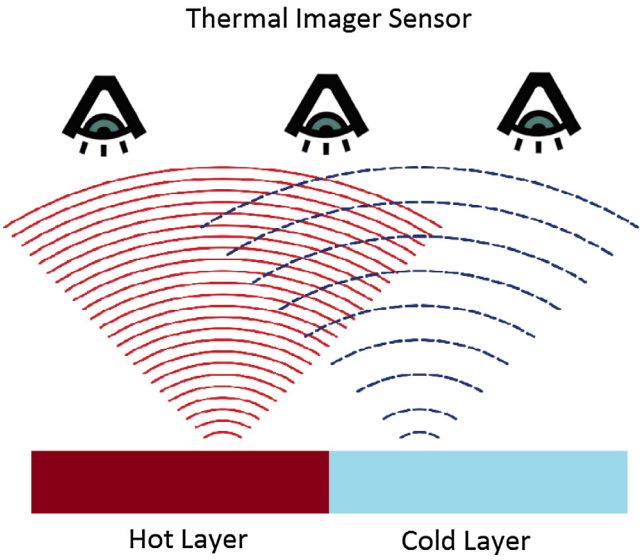

Fig. 21. Thermal imager artifact: reading a mix of infrared frequencies when trying to capture a step function temperature profile in a composite assembly.

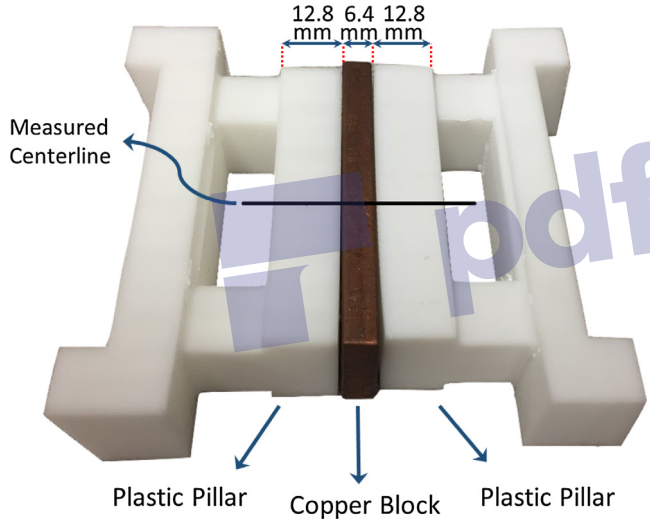

Fig. 22. Experiment for assessing the accuracy of the thermal imager when reading a step function temperature profile.

imager is logging temperature data from the plastic pillars at 8 frames/s when the copper block is added to the set up immediately after removing it from an ice container and tightened between the plastic pillars. The resulting structure has a known step function in temperature profile.

Fig. 23 shows the result of the thermal imager's measurement versus the predicted actual temperature profile at $t = 0$ s. The smooth transition at the boundaries of the plastic pillars and copper block shows the measurement artifact due to thermal imager inability to measure an abrupt change in temperature profile (see Fig. 24).

Using the same geometry of composite assembly and material properties presented in Fig. 4, a transient finite element analysis was performed using ANSYS MAPDL. The results are compared with those from the MC simulation for the transition area at $t = 20$ s. The initial condition is defined as a rectangular area in the middle of the copper plate with side length = 10 cm at the temperature of 360 K, while rest of the plate is at temperature = 300 K. Fig. 22 shows the agreement between results of both numerical

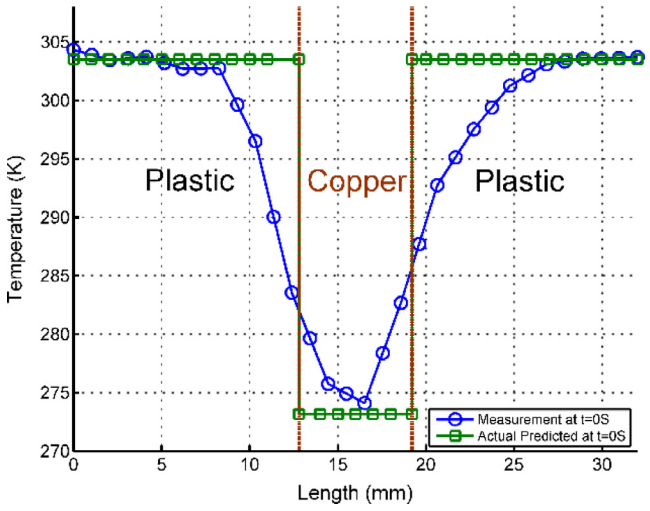

Fig. 23. Experiment for assessing the accuracy of the thermal imager when reading a step function temperature profile – results.

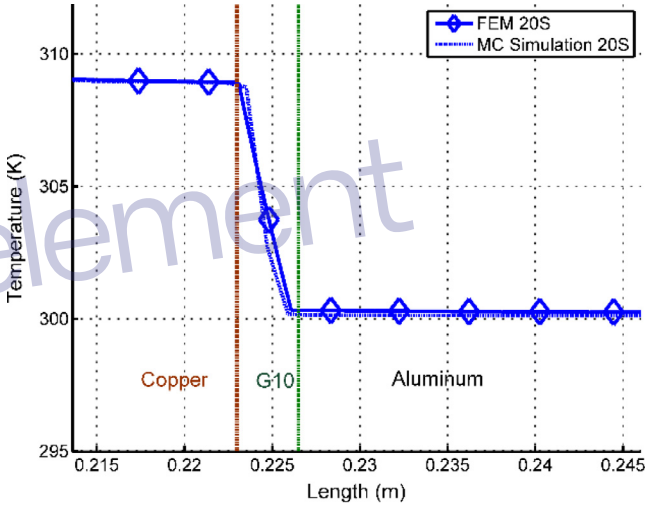

Fig. 24. MC simulation vs. a finite element simulation for the composite assembly experiment.

methods and verifies the ability of the proposed MC simulation to predict the temperature profile transition in composite layered structures.

7. Conclusions

A novel mesh-free Monte-Carlo method for two-dimensional transient heat conduction in composite media with temperature dependent thermal properties has been presented. The transient conductive heat transfer is simulated by finding the temperature of any test point (sink) by receiving energy packages (particles) that are randomly arriving from the vicinity (source) of the point. The thermal diffusivities along the particle's path from source to sink are taken into account. It has been shown that even small numbers of particles emitted from each point yields accurate result with less than one percent error.

Haji Sheikh and Sparrow [7] introduced the Monte-Carlo solution of transient heat conduction based on Bessel functions relating time and step length for each particle's floating random walk. Their method calculates the temperature of each point by simply averaging the particles' temperature emitting from the respective point,

and is applicable to homogenous media. Burmeister [16] reported the floating random walk Monte-Carlo approach to tackle steady state heat conduction problems in composite media with temperature dependent material properties. The study presented in this paper proposes modifications in both methods and combines them to address transient heat conduction in composite media with temperature dependent thermal diffusivities. Results from the proposed approach have been successfully compared against both FEM results and measurements acquired in experiments using a thermal imaging device.

References

[1] N. Metropolis, S. Ulam, The Monte Carlo method, J. Am. Stat. Assoc. 44 (247) (1949) 335–341.

[2] J.R. Howell, Application of Monte Carlo to heat transfer problems, 1969, pp. 1–54.

[3] A. Maurente, F.H.R. França, A Multi-Spectral Energy Bundle method for efficient Monte Carlo radiation heat transfer computations in participating media, Int. J. Heat Mass Transf. 90 (2015) 351–357.

[4] H.L. Yi, C.H. Wang, H.P. Tan, Transient radiative transfer in a complex refracting medium by a modified Monte Carlo simulation, Int. J. Heat Mass Transf. 79 (2014) 437–449.

[5] Z. Shomali, B. Pedar, J. Ghazanfarian, A. Abbassi, Monte-Carlo parallel simulation of phonon transport for 3D silicon nano-devices, Int. J. Therm. Sci. 114 (2017) 139–154.

[6] Q. Li, W. Ye, An interfering Monte Carlo method for partially coherent phonon transport in superlattices, Int. J. Heat Mass Transf. 107 (Apr. 2017) 534–543.

[7] F. Gong et al., Effective thermal transport properties in multiphase biological systems containing carbon nanomaterials, RSC Adv. 7 (22) (2017) 13615–13622.

[8] F. Gong, K. Bui, D.V. Papavassiliou, H.M. Duong, Thermal transport phenomena and limitations in heterogeneous polymer composites containing carbon nanotubes and inorganic nanoparticles, Carbon N. Y. 78 (2014) 305–316.

[9] H.M. Duong, D.V. Papavassiliou, L.L. Lee, K.J. Mullen, Random walks in nanotube composites: Improved algorithms and the role of thermal boundary resistance, Appl. Phys. Lett. 87 (1) (2005) 1–4.

[10] A. Haji-Sheikh, E.M. Sparrow, The floating random walk and its application to monte carlo solutions of heat equations*, SIAM J. Appl. Math. 14 (2) (1966) 370–389.

[11] R. Bahadori, H. Gutierrez, S. Manikonda, R. Meinke, Monte Carlo method simulation for two-dimensional heat transfer in homogenous medium and proposed application to quench propagation simulation, IEEE Trans. Appl. Supercond. 27 (4) (2017) 1–5.

[12] L.C. Burmeister, The effect of space-dependent thermal conductivity on the steady central temperature of a cylinder, J. Heat Transfer 124 (1) (2001) 195–197.

[13] F. Gong, D.V. Papavassiliou, H.M. Duong, Off-lattice Monte Carlo simulation of heat transfer through carbon nanotube multiphase systems taking into account thermal boundary resistances, Numer. Heat Transf. Part A Appl 65 (June 2015) (2014) 1023–1043.

[14] V. Sizyuk, A. Hassanein, Efficient Monte Carlo simulation of heat conduction problems for integrated multi-physics applications, Numer. Heat Transf. Part B Fundam. 66 (5) (2014) 381–396.

[15] A. Haji-Sheikh, Application of Monte Carlo Methods to Thermal Conduction Problems, University of Minnesota, 1965.

[16] J.Y.M.W.J. Minkowycz, E.M. Sparrow, Handbook of Numerical Heat Transfer, second ed., Wiley, Hoboken, New Jeresey, 2006.

[17] F. Kowsary, S. Irano, Monte Carlo solution of transient heat conduction in anisotropic media, J. Thermophys. Heat Transf. 20 (2) (2006) 342–346.

[18] P. Chiovaro, P.A. Di Maio, On the adoption of the Monte Carlo method to solve one-dimensional steady state thermal diffusion problems for non-uniform solids, Appl. Math. Model. 37 (23) (2013) 9707–9721.

[19] I.V. Belova, G.E. Murch, T. Fiedler, A. Öchsner, The Lattice Monte Carlo method for solving phenomenological mass and thermal diffusion problems, Diffusion-Fundam. 4 (Lmc) (2007) 13–22.

[20] T. Fiedler, I.V. Belova, A. Rawson, G.E. Murch, Optimized Lattice Monte Carlo for thermal analysis of composites, Comput. Mater. Sci. 95 (2014) 207–212.

[21] L. Farnell, W.G. Gibson, Monte Carlo simulation of diffusion in a spatially nonhomogeneous medium: correction to the Gaussian steplength, J. Comput. Phys. 198 (1) (2004) 65–79.

[22] L. Farnell, W.G. Gibson, Monte Carlo simulation of diffusion in a spatially nonhomogeneous medium: a biased random walk on an asymmetrical lattice, J. Comput. Phys. 208 (1) (2005) 253–265.